

## Blazed Diffraction Gratings on Si — First Results

© L.I. Goray,<sup>1,2</sup> T.N. Berezovskaya,<sup>1,3</sup> D.V. Mokhov,<sup>1</sup> V.A. Sharov,<sup>1,3</sup> K.Yu. Shubina,<sup>1</sup> E.V. Pirogov,<sup>1</sup>  
A.S. Dashkov<sup>1</sup>

<sup>1</sup> Alferov University,  
St. Petersburg, Russia

<sup>2</sup> Institute for Analytical Instrumentation,  
St. Petersburg, Russia

<sup>3</sup> Ioffe Institute,  
St. Petersburg, Russia  
e-mail: lig@pcgrate.com

Received March 26, 2021

revised March 26, 2021

accepted March 26, 2021

Using direct laser lithography and wet etching of polished vicinal Si(111) wafers, a technology was developed and diffraction gratings 500 grooves/mm with a blaze angle of  $4^\circ$  were fabricated. The manufacturing process of a reflective Si-grating with the triangular profile (sawtooth) can be divided into four main steps: (1) obtaining a pattern of a protective mask for grooves etching; (2) anisotropic etching of grooves in KOH solution; (3) etching to smooth the grating profile and polish the surface of working facets; (4) coating to increase reflectivity. The samples obtained were characterized using scanning electron microscopy and atomic force microscopy methods to determine the shape of the groove profile and roughness: the shape turned out to be close to the ideal triangular, and the RMS roughness was less than 0.3 nm. Using PCGrate<sup>TM</sup> software and taking into account the measured real groove profile, the diffraction efficiency of gratings operating in classical and conical mounts in soft-X-ray and extreme ultraviolet radiation has been simulated. The obtained efficiency values are close to the record ones for the corresponding spectral range and the Au-coating of the grating.

**Keywords:** diffraction grating, wet etching technology of Si, sawtooth groove profile, AFM, SEM, diffraction efficiency modelling.

DOI: 10.21883/TP.2022.13.52229.81-21

### Introduction

For mid-frequency and high-frequency diffraction gratings the classical (in-plane) diffraction gives the acceptable values of the working order efficiency only in the soft-X-ray (SXR) and extreme ultraviolet (EUV) ranges [1]. However, the mount of grazing-incidence conical (off-plane) diffraction has large advantages in efficiency when such gratings are used in short-wave regions of the X-ray range (hard X-ray and „tender X-ray“), including high orders, and for achieving the high dispersion and resolution. In this mount the unprecedented diffraction efficiency, close to the mirror reflectance, can be achieved for sawtooth gratings with blaze angles of several degrees, which are much easier to manufacture. For theoretical analysis of such gratings efficiency, the numerical calculations based on the rigorous electromagnetic theory of diffraction are required [2].

The developed method of manufacturing the diffraction gratings with non-symmetrical grooves profile using wet etching was used for visible radiation on substrates of GaAs semiconductor crystals [3] and on Si — for infrared [4] and X-ray radiation [5]. Wet etching is also used for manufacturing the holographic gratings based on exposed films of arsenic sulfide [6]. Advantages of anisotropic wet etching of misoriented by several degrees Si(111) substrates for obtaining the low-roughness high-frequency

gratings with relatively large blaze angles by optimizing the technological process were demonstrated in [7]. In this study, we describe the important features of the developed technology of X-ray blazed gratings manufacturing on Si substrates and the results of scanning electron microscopy (SEM)/atomic force microscopy (AFM) studies of the surface relief and roughness of similar gratings, as well as calculations of their efficiency using PCGrate<sup>TM</sup> software [8] and measured groove profiles.

### 1. Gratings manufacturing technology

The process of manufacturing the reflecting Si grating with the triangular profile (sawtooth grating) can be conveniently divided into four main stages: (1) obtaining a pattern of a protective mask for grooves etching; (2) anisotropic etching of grooves in KOH solution; (3) etching to smooth the grating profile and polish the surface of the reflecting (working) facets; (4) coating to increase reflectivity. In turn, each stage consists of several operations, that will be examined in detail.

For application of material and obtaining a pattern of the protective mask, selection of etching conditions and method of surface cleaning from silicon etching products, studying the etchants for profile smoothing and surface

polishing, the crystallographic orientation of a substrate is not important. This is important only for obtaining the triangular (sawtooth) grooves profile. Therefore, because of high availability of Si substrates (100), compared with rarer and more expensive Si substrates (111) with misorientation by several degrees, for development of some operations and stages of the reflective grating manufacturing process the former ones were used at initial stages.

### 1.1. Protective mask obtaining for grooves etching in KOH

SiO<sub>2</sub> or Si<sub>3</sub>N<sub>4</sub> [9], and chromium [10] lately are widely used as the protective mask material for silicon etching in KOH solutions. A Cr mask is obtained by reactive ion etching through the organic resist mask [10] or using metallization lift-off technique [11]. For the stoichiometrical Si<sub>3</sub>N<sub>4</sub> formation the low-pressure chemical vapor deposition (LPCVD) [12] or chemical vapor deposition (CVD) method [7] is used. We applied the layer of stoichiometrical Si<sub>3</sub>N<sub>4</sub> using the low-temperature plasma enhanced chemical vapor deposition (PECVD) at an Oxford Instruments™ PlasmaLab 100. Using plasma chemistry it is possible to obtain dielectric films of nanosized thicknesses with good quality, chemical purity, high adhesion, homogeneous in composition and thickness.

To obtain Si<sub>3</sub>N<sub>4</sub> and Cr masks we developed a wet etching technology, remarkable for its low cost and design simplicity: the Cr mask was etched in a cerium etchant through the organic photoresist mask (PR mask), the Si<sub>3</sub>N<sub>4</sub> mask was etched in BHF through the PR or Cr mask. Based on experimental results we chose the Cr mask due to its chemical resistance to HF and KOH solutions, as well as due to lesser labor intensity, lesser duration and better reproducibility of its manufacturing method. To form the Cr mask the layer of Cr with the thickness of ~ 25 nm was applied on a cleaned Si substrate using electron-beam evaporation with the continuous rotation of samples at a BOC Edwards™ AUTO 500; the layer thickness was profilometrically controlled. Usually, for a grating topological pattern application on Si substrate the interference [13] or electron-beam [14] lithography is used; for manufacturing a mid-frequency grating we used the direct write laser (DWL) lithography [15]. Photoresist AZ 701 MiR was applied to the layer of Cr by centrifugation, and the topological pattern was drawn with the laser beam at a laser lithography unit Heidelberg™ DWL 66FS. The PR mask pattern was developed in a developer AZ 726 MIF. To obtain the protective Cr mask, the sample with PR masks was etched in the cerium etchant, after which the photoresist was removed by boiling in acetone.

### 1.2. Anisotropic grooves etching in KOH

Before etching the grooves pattern directly in Si, the surface of samples should be cleaned from the native layer

of SiO<sub>2</sub> on a surface, for which we used a solution of HF:H<sub>2</sub>O (1:3).

To transfer the grating pattern directly to silicon wafer, it is etched in the potassium hydroxide (KOH) solution with various concentrations at temperatures from room to 50°C with thorough mixing of the solution [7,16]. KOH etches the surfaces of {111} slower, than the rest silicon, that results in angular facets with facet inclination, defined by orientation of surfaces of {111} against the substrate plane. Therefore, KOH etches the grooves pattern in Si, simultaneously setting the blaze angle of grating facets. We chose the anisotropic etching at a room temperature in water solution of KOH with the concentration of 20 wt.%. The detailed development of the process was performed for determination of a perfect combination of mixing methods, modes and durations of etching.

The authors of [7] have not specified what they meant by „thorough mixing of the solution“. That can be a mixing using a magnetic stirrer bar, or a mechanical rotating stirrer, or air or nitrogen agitation, ultrasound. Without the mixing, the etching is very non-homogeneous. We made experiments on etching with the mixing using the magnetic stirrer with variations of the rotation speed, bar size, vessel form and diameter, KOH solution volume, sample orientation (vertical or horizontal), grooves orientation against the etching solution flow (along or across). Also we made experiments on etching with mixing using ultrasound (US), varying the vessel size, KOH solution volume, location of sample and grooves orientation (vertical or horizontal). We observed that mixing conditions during etching influence not only on speed and uniformity of etching, but also a working facet surface roughness. As an illustration, Fig. 1 shows SEM images of the sample surface after etching in KOH with the mixing using the magnetic stirrer with the vertical sample location and grooves orientation along an etchant flow (Fig. 1, *a*) and using the US mixing with various locations of the sample (Fig. 1, *b, c*).

We chose the ultrasonic mixing, with which the best results in terms of the surface roughness and etching uniformity were obtained; after grooves etching in KOH we removed the chrome mask in the cerium etchant.

### 1.3. Smoothing and polishing etching

Prolonged exposure of KOH leads to a lateral etching of silicon under the mask (undercutting under the mask), resulting in the formation of silicon nubs on top. To prevent shading of the adjacent facets by Si nubs, reducing the blazed facet length and interfering the atomic flow during the reflecting layer deposition, they should be removed, for which the smoothing etching is performed. To reduce the blazed facet roughness the polishing etching is performed.

#### 1.3.1. Smoothing etching

To smooth the grating profile by etching the Si nubs without the grating quality degradation, the etchant and

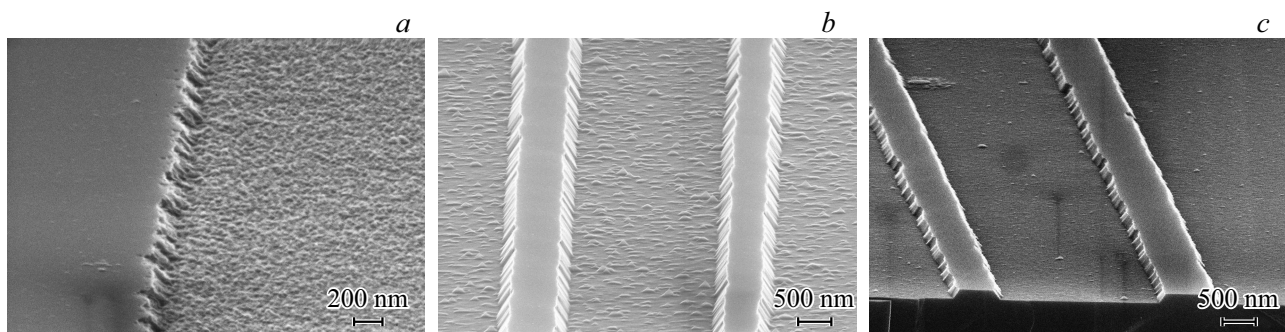


**Figure 1.** SEM images (magnification of 50 000 $\times$ ) of surface after etching in KOH using: *a* — the magnetic stirrer, vertical sample, groove along the etchant flow; the US mixing, sample location: *b* — horizontal; *c* — vertical.

modes should be selected. Smoothing etchant should primarily remove the raised profile areas (Si nubs), while the reflecting facet inclination angle should remain the same, and reflecting facet surface roughness should not deteriorate. The authors of [7] tried the thermal wet oxidation of silicon at a temperature of 800 $^{\circ}$ C with the following oxide etching in 49% HF for the Si-nubs removal, but this method resulted in significantly bent facets, therefore it was rejected. They achieved the best result in the Si-nubs removal at a multi-stage procedure of the chemical oxidation in a piranha solution, alternating with the grown oxide etching in HF. However, after such treatment there were serious surface defects in the form of nanosized pits with width of 30–50 nm and depth of several nanometers. In the study [17] the multi-stage procedure of repeated nine cycles of RCA-1/HF treatment is also applied for the removal of any irregularities and roughness obtained after the KOH etching. The authors of [4] perform small isotropic etching (etchant composition is not specified) for the removal of silicon nubs and obtaining the required profile.

After trying various etchants we succeeded in finding the one that etches Si-nubs without changing the inclination angle and without deteriorating the working facet roughness. The main etching parameter, influencing the profile shape and length of the working facet of Si grating, is etching duration. Properly selected duration of the smoothing etching provides the perfect triangular shape of grating and maximum possible length of the working facet. We made experiments with the selected etchant to define the rate of the Si-nubs etching and study the influence of the etching modes and duration on Si-grating profiles and roughness of the working facet. The Si-nubs height is varied from 18 to 72 nm, for their removal the smoothing etching takes from 60 to 180 s. Fig. 2 shows SEM images of a transverse cleavage of Si grating samples before and after smoothing etching. Si-nubs are observed immediately after the anisotropic etching in KOH (Fig. 2, *a*), after the smoothing etching with the non-sufficient duration (Fig. 2, *b*) and not observed after the smoothing etching with the sufficient (Fig. 2, *c*) and excess (Fig. 2, *d*) durations.

Not completely removed Si-nubs (Fig. 2, *b*) reduce the reflecting facet length, resulting in the efficiency reduction (reflectivity) of the Si grating. An excess smoothing, appearing in the excess rounding of the profile (Fig. 2, *d*), also results in the working facet length reduction. Thus, it is necessary to find the balance in the smoothing etching (Fig. 2, *c*) between desire to maintain the largest working facet and the necessity to completely remove Si-nubs. In smoothing etching, the main criterion for choosing the duration of etching is the completeness of the Si-nubs removal.

### 1.3.2. Polishing etching

As mentioned earlier, the authors of [17] use a nine-cycle RCA-1/HF treatment to remove any irregularities and roughness, i.e., perform simultaneously smoothing and polishing etching, and they report on submicron roughness. In the very beginning of our development the RMS of the reflecting facet roughness immediately after anisotropic etching in KOH was in a range from 1.8 to 4.9 nm, that is absolutely unacceptable. After optimization of modes of etching in KOH the RMS of the reflecting facet roughness reduced to 0.45–1.36 nm, that is better, but still unacceptable. To reduce the reflecting facet roughness several etching agents were tried: piranha solution, peroxide ammonia solution (RCA-1), tetramethylammonium hydroxide (TMAH), acid etchant for slow isotropic silicon etching HF:HNO<sub>3</sub>:H<sub>2</sub>O. Table 1 contains the results of treatment in various etchants of sample surfaces, cutted from the same grating immediately after the anisotropic etching in KOH. In Table 1, line 3, it can be observed that sample is over-etched in the smoothing etchant, however the triangular profile and inclination are still on the most part of the working facet, and only on the length of 190–200 nm there is an even, smooth silicon surface. It is due to the fact that for the Si-nub with the height of 35 nm the duration of smoothing etching of 280 s turned out twice longer than the required one ( $\sim$  130 s). However, it is important that the smoothing etchant does not deteriorate the surface roughness.

For the following optimization of polishing etching modes the etchants TMAH and HF:HNO<sub>3</sub>:H<sub>2</sub>O were selected.

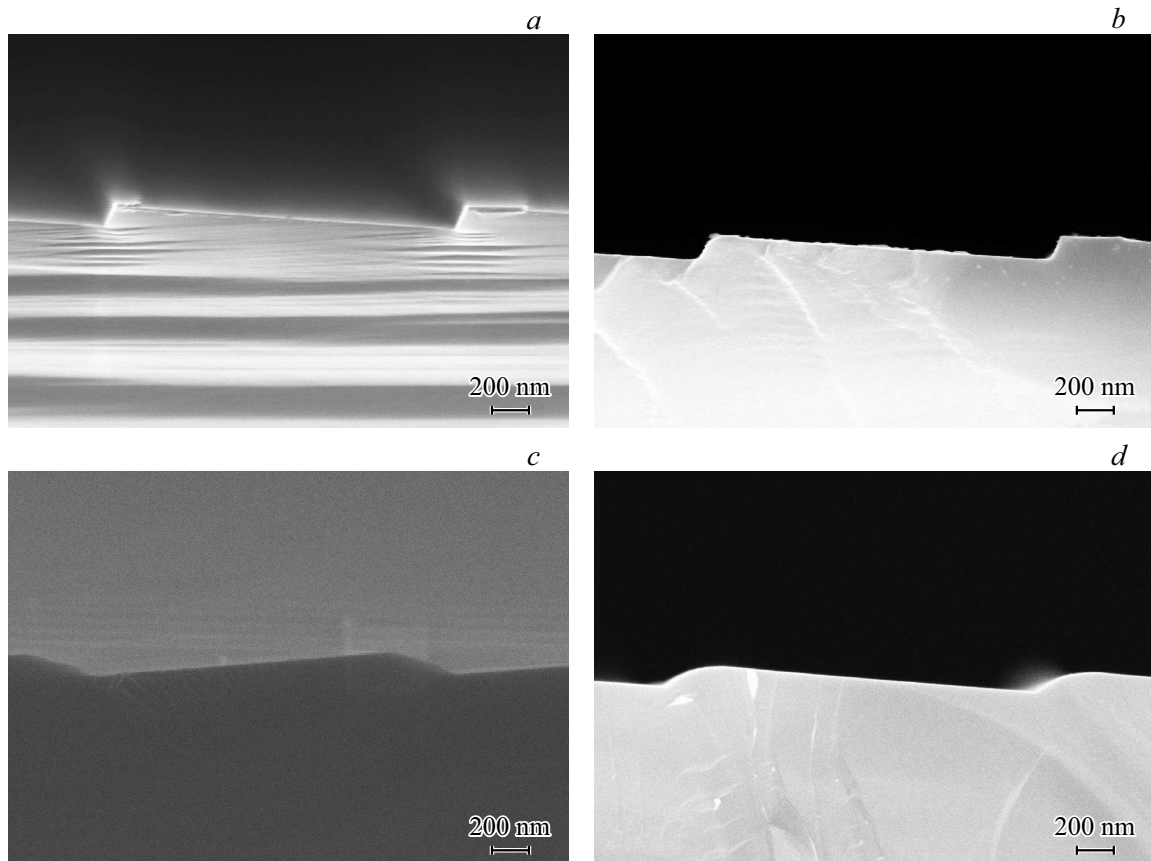


**Figure 2.** SEM images (magnification of 100 000 $\times$ ): *a* — after anisotropic etching in KOH, height of Si-nubs is 48 nm; *b-d* — after smoothing etching with various durations.

Polishing should not deform the grating profile (length and inclination angle of the reflecting facet, groove depth), therefore AFM studies are required at a polishing etchant optimization.

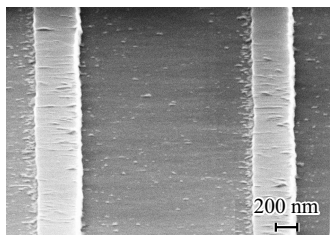
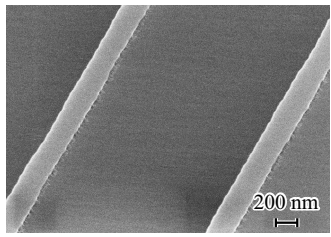
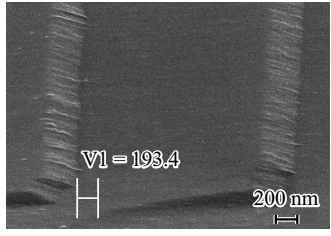
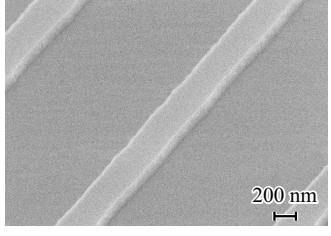
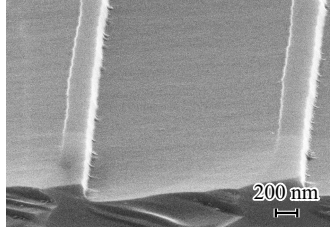
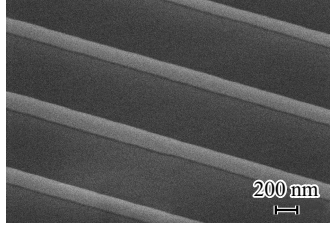
#### 1.4. Application of reflecting coating

Coating of a single- or multi-layer material is applied to Si gratings with the triangular profile designed for the spectral range of soft and hard X-ray radiation to improve the reflectivity. Reflecting coatings are usually applied by magnetron or ion beam sputtering [7,18,19]. Mo, Ru, Zr [16], as well as Au or other noble metals with a sub-layer of Cr or Ti for an adhesion improving [4,12,17,20] are used most frequently. Various multi-layer coatings, consisting of a pair of more and less absorbing materials and allowing to increase the reflection coefficient and/or grazing angle, that is very important in this spectral range, are also widely used [21]. However, deposition of coatings, consisting of several dozens or even hundreds of bilayers, may result in degradation of grating layer boundaries and materials intermixing, i.e., to changes in its diffraction properties, which should be taken into account [18,22,23].

The coating quality criteria are the following: the reflectivity, the surface roughness, without the Si-grating

profile deformation (the reflecting facet inclination angle, the reflecting facet length, the triangular groove profile, the groove depth). For the optimization of Si-gratings manufacturing technology, the simplest coating of Cr/Au (5/15 nm) was selected and formed at the vacuum coater BOC Edwards™ AUTO 500: the layer of Cr was applied on rotating samples using the electron-beam evaporation, and the layer of Au — using both electron-beam and thermal vacuum evaporation methods. In the first experiment the coating was applied on a fragment of the initial clean Si substrate, in the second experiment — on two samples of the same Si grating with the smoothed profile and various grooves orientation against the metal flow. In both cases the results were unsatisfactory. Parameters of the thermal vacuum deposition should be varied further: 1) the sample temperature; 2) deposition with and without rotation (more likely, with rotation, since it allows to improve the homogeneity of a metal distribution over the surface); 3) the sample location relating to the sources (since positions of the electron-beam source and the thermal evaporation source are different relatively to the radius (center) of the sample holder and the evaporated metal flow shape is conical, it is necessary to define the distance from the center that gives the best result in terms of the homogeneity of the film thickness and surface roughness);

**Table 1.** Polishing etching of samples of diffraction Si grating

Sample	Roughness of reflecting facet, RMS, nm	Chemical treatment	SEM image, magnification 100 000×
1	Not measured	KOH	
2	0.367	KOH, piranha solution	
3	0.353	KOH, smoothing etching	
4	0.319	KOH, TMAH	
5	0.608	KOH, RCA-1	
6	0.343	KOH, HF:HNO <sub>3</sub> :H <sub>2</sub> O	

4) the orientation of Si-grating grooves relative to the flow, including the sample inclination. In the third experiment the coating was applied on a fragment of the Si-substrate

and on the sample of Si-grating with the smoothed profile. The results of three experiments of the coating application are presented in Table 2 which demonstrates the improved

**Table 2.** Results of the first Cr/Au coating sputtering experiments

№ of experience	Sample	Surface roughness, RMS, nm		Note
		Without coating	With coating of Cr/Au	
1	Si substrate	0.152	1.923	1) Without sample heating in chamber 2) Without sample rotation
2	Si grating	0.340	2.859	1) Different samples orientation against metal flow 2) Samples heating in chamber 3) Samples rotation 4) Application of Cr and Au using electron-beam evaporation 5) Due to small amount of Cr in crucible it is possible that thickness of layer of Cr < 5 nm, poor adhesion of Au
	Si grating		2.357	
3	Si substrate	0.194	0.744	1) Samples heating in chamber 2) Samples rotation 3) Electron-beam evaporation of Cr 4) Thermal vacuum evaporation of Au
	Si grating	0.278	1.335	

surface roughness in the third experiment compared to the previous experiments for Si substrate (in 2.6 times) and Si grating (in 1.8 times), but still unsatisfactory and much worse than for the initial sample. Until the surface roughness of  $RMS \leq 0.5$  nm is not obtained on the Si substrate, there is no point to perform AFM studies of the profile change and random roughness of grooves after the coating application.

## 2. Grooves metrology

The surface morphology control is required at each stage of the Si grating manufacturing. SEM images are used only at process optimization stages, since a fragment is cut out of the sample to make a cross-cut split (CS). However, the SEM analysis is fast and sufficiently accurate to define the main geometrical parameters of groove profiles and to make a choice between „high quality“ and „low quality“ (with the deformed profile shape, small working facet length, high roughness and residues of etching and treatment products). AFM studies are non-destructive and suitable also for roughness measurements. The comparison of SEM and AFM images of grating samples shows the quantitative correspondence of the observed results.

Fig. 3 shows examples of the SEM images of the diffraction Si-grating sample with the triangular profile with the period of  $2\mu\text{m}$  manufactured using etching through the protective Cr mask of the Si substrate (111) $4^\circ$ , with the following smoothing. Pictures were made at various magnifications ( $100\,000\times$  and  $50\,000\times$ ) and at various systems, Zeiss Supra 25 and JEOL JSM 7001F, respectively. The overview (panoramic) SEM images were obtained at a magnification of  $10\,000\times$  at the both devices.

According to the analysis of SEM images, the grooves surface is uniform, even, without visible irregularities.

Overall, the grooves profile geometry is close to perfect triangular. After the etching, the nub with the height of 70 nm (left pictures) remains, but it is completely removed at the smoothing stage (see right pictures). The average length of the working facet is  $\sim 1800$  nm that corresponds to the average inclination angle of the non-working facet of  $\sim 30\text{--}35^\circ$ , that is a good parameter for such short-wave gratings with the low blaze angle.

Fig. 4 shows the AFM scans of the diffraction Si-grating sample with the triangular profile with the period of  $2\mu\text{m}$  and the average length of the working facet of  $\sim 1750$  nm manufactured using etching through the protective Cr mask. Our studies were performed at an atomic-force microscope NT-MDT NTegra Aura [24] in the semicontact (or tapping) mode; there were  $512 \times 512$  points in all scans. We used silicon probes made by TipsNano<sup>TM</sup> with the typical bending radius of  $\sim 6$  nm. Fig. 4 (left) shows the AFM scan of a long  $10\mu\text{m}$  surface of the Si-grating sample of 500 grooves/mm and the topogram of the working facet inclination angle; Fig. 4 (right) shows the AFM-measured surface of this grating. The root-mean-square deviation of the roughness, as per measurements data, was 0.28 nm in the field of  $1 \times 1\mu\text{m}^2$ .

## 3. Diffraction efficiency calculations

For rigorous calculations of the diffraction efficiency of the studied gratings considering AFM-measured actual grooves profile and random roughness we used PCGrate<sup>TM</sup>-SX v.6.7 code [8] based on the rigorous method of boundary integral equations [2]. Using this software we simulated efficiencies of the manufactured gratings with realistic (polygonal) groove profiles and observed that it can reach 30% in SXR-EUV and 50–70% in HXR ranges in classical and conical mounts, respectively. The

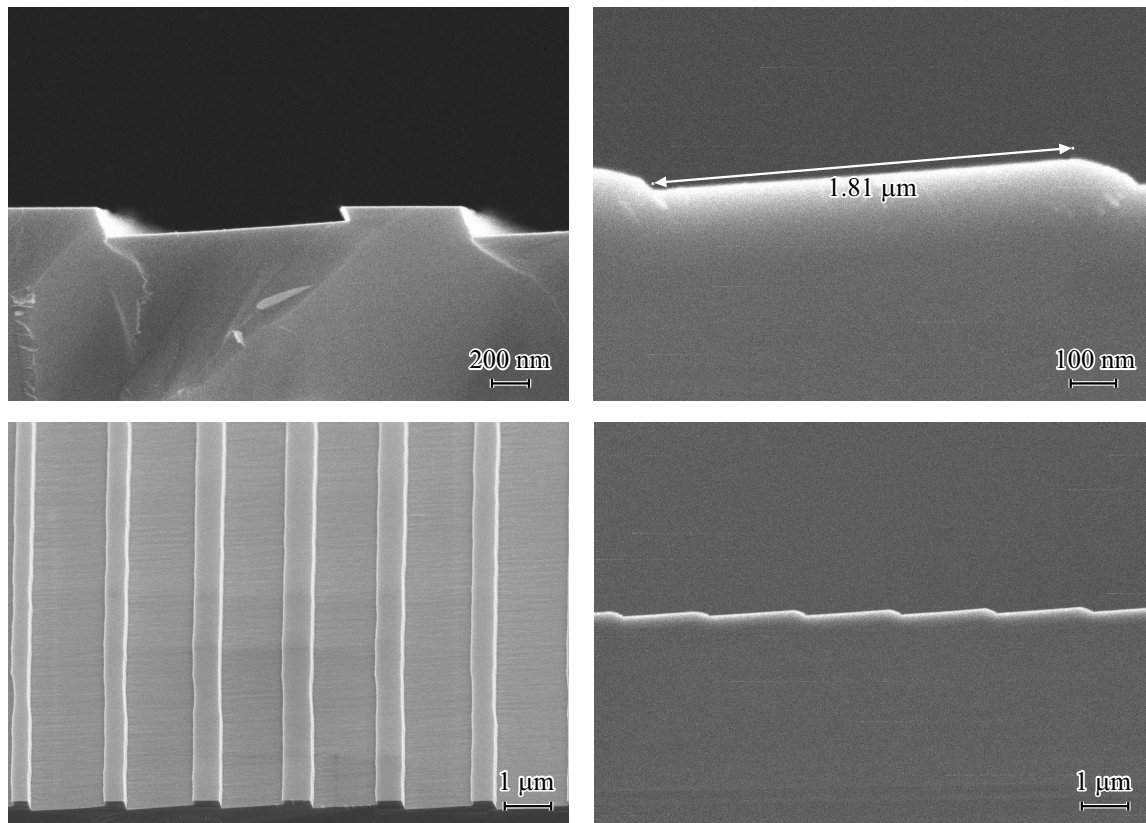


**Figure 3.** SEM images observed: left — after etching in KOH at a magnification of 100 000 $\times$  at the Zeiss Supra 25; right — after a smoothing etching for 120 s at a magnification of 50 000 $\times$  at the JEOL JSM 7001F. Reflecting facet length is  $\sim 1825$  nm (50 000 $\times$ ). Overview (panoramic) SEM images are obtained at a magnification of 10 000 $\times$  at the both devices.

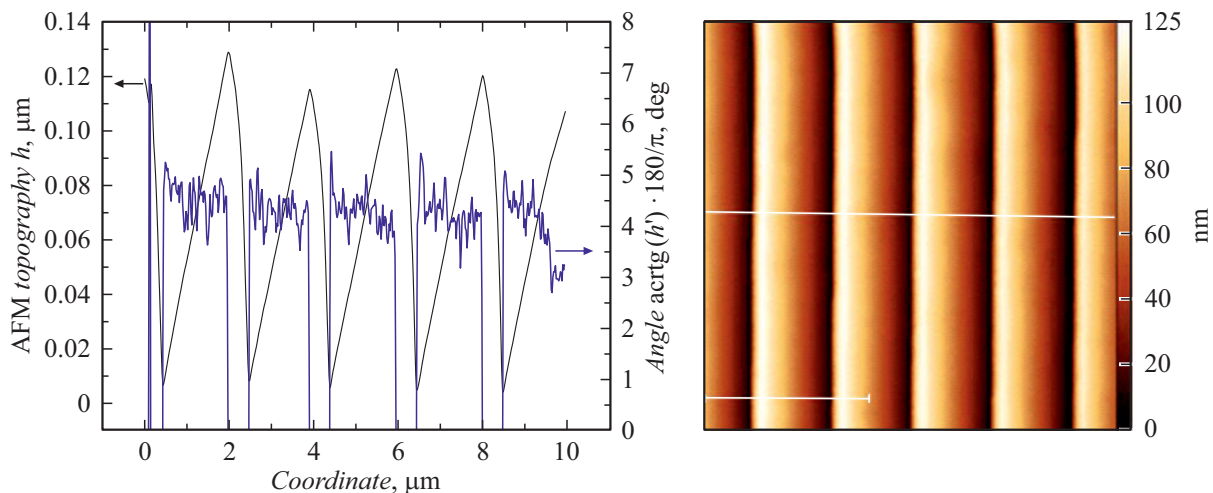


**Figure 4.** Left — AFM scan of a  $10\ \mu\text{m}$  surface of the Si-grating sample of 500 grooves/mm and topogram of the reflecting facet inclination angle; right — AFM scan of a  $10 \times 10\ \mu\text{m}^2$  surface of the Si-grating sample.

averaged groove profile obtained from the AFM data for one of the manufactured gratings was used for rigorous calculations of diffraction orders efficiencies depending on the incidence angle and wavelength in the SXR–EUV range.

Fig. 5 shows the results of rigorous calculations of the efficiency of such Au grating in classical mount of diffraction

at the incidence angle of  $83^\circ$  and wavelength range of 7–25 nm for orders with numbers from minus 6th to 0. As it can be observed from the diagrams, the curves of the diffraction efficiency of orders from minus 6th to minus 2nd sequentially cover the whole examined spectral range and have the maximums near 30% that is unprecedented for

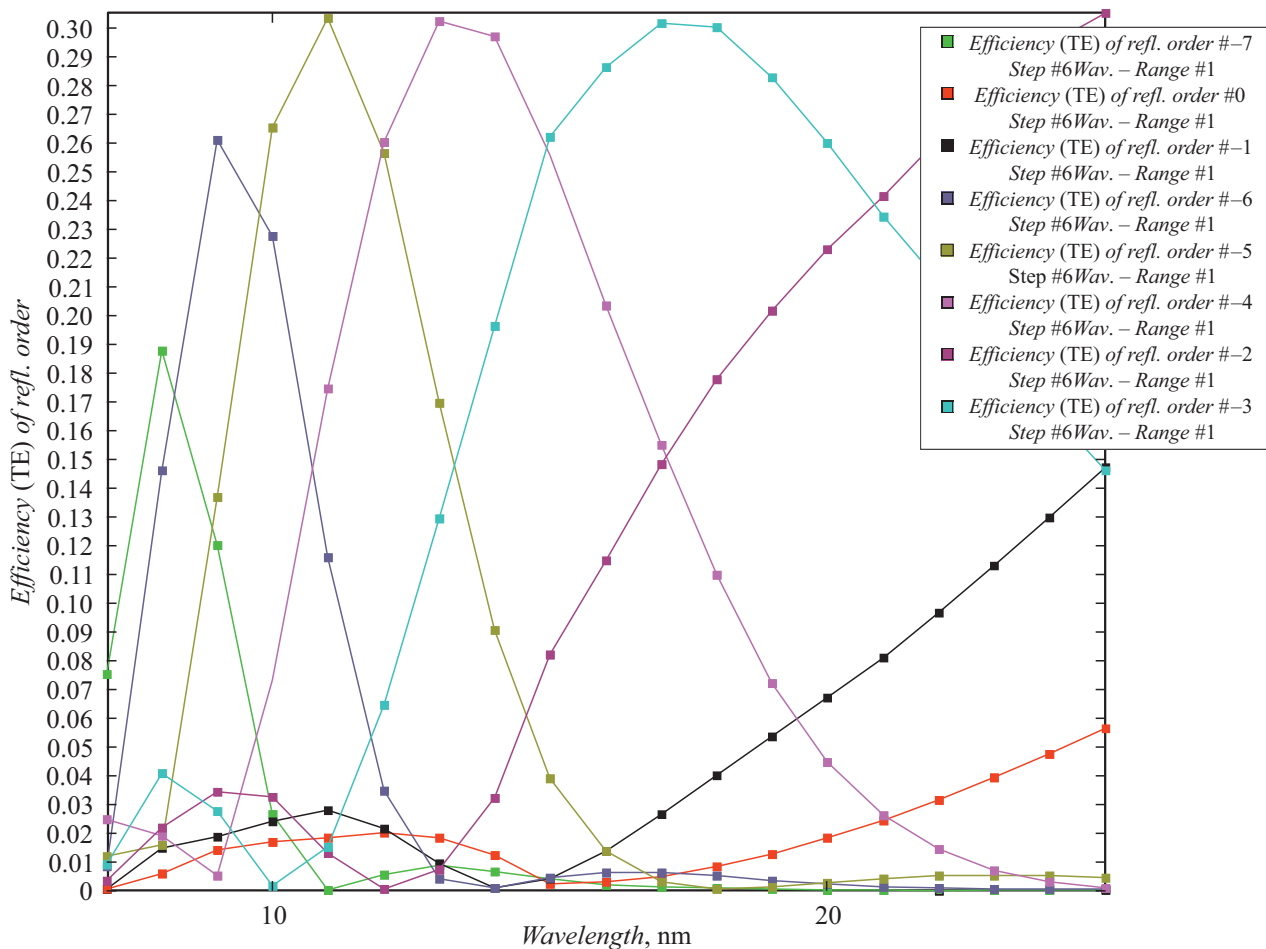


**Figure 5.** Theoretical diffraction efficiency of orders of the Au grating of 500 grooves/mm in the classical mount, calculated at an incidence angle of  $83^\circ$  using the actual groove profile, on wavelength.

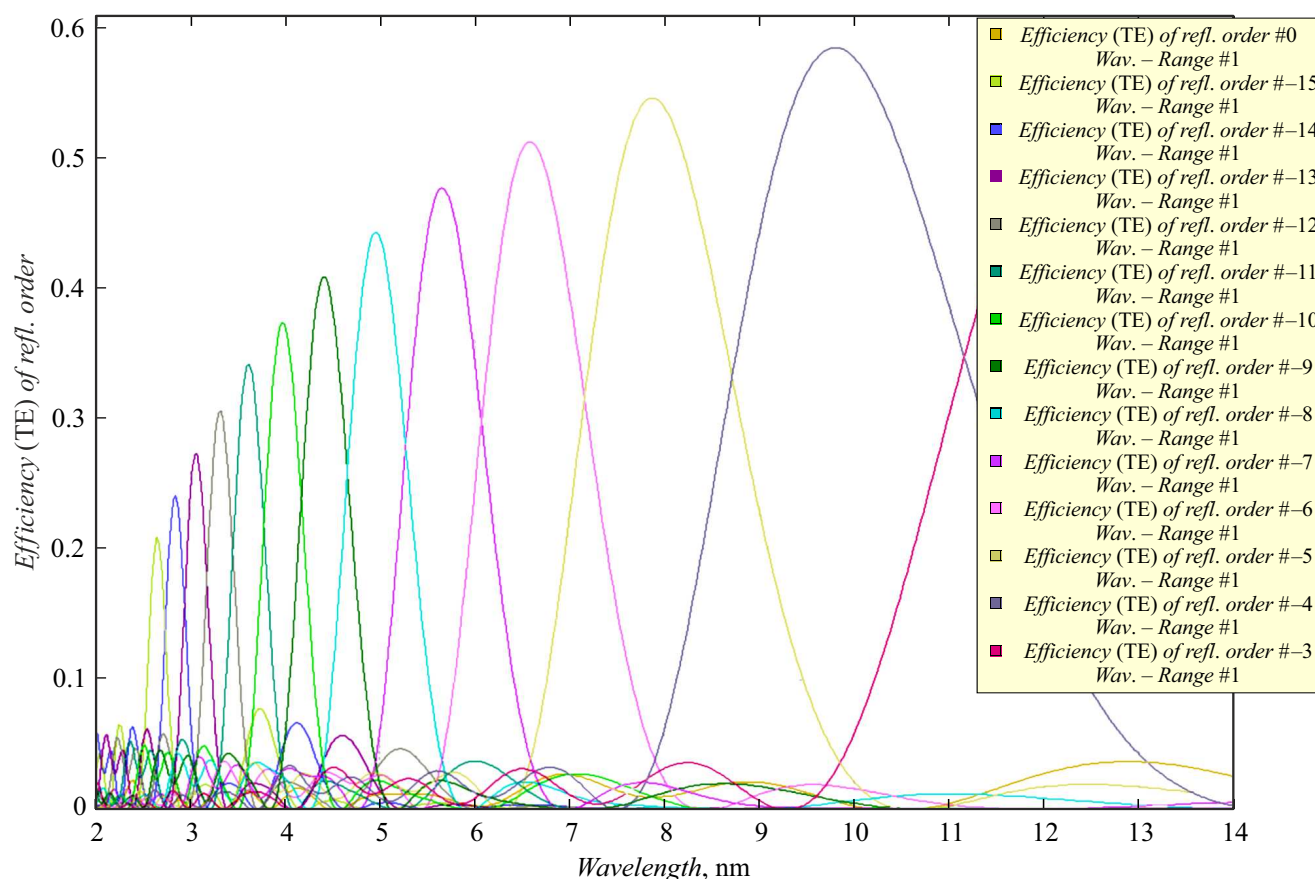
an Au-coated grating in the indicated spectral range and classical diffraction mount. It should be noted that the maximum diffraction efficiency of a grating with the perfect triangular profile is just a several percentages higher. At the same time, the efficiency of order 0 of the grating with the realistic profile shape is low and in the wavelength range of 7–20 nm is  $\sim 1\%$  in average that also indicates the good „blaze“ of the grating, i.e., the almost perfect triangular profile.

Fig. 6 shows the results of efficiency calculations for the same Au grating operating in the conical diffraction mount at a polar incidence angle of  $4^\circ$  and azimuthal incidence angle of  $82^\circ$ , depending on wavelength in the SXR range. As it can be observed from the diagrams, the curves of the diffraction efficiency of orders from minus 15th to minus 3rd sequentially (from left to right) cover the whole examined range from 2 to 14 nm and have the maximum near 60%, that is an absolute record for an Au-coated grating in the examined spectral range. It should be noted that the maximum diffraction efficiency of a grating with the perfect triangular profile is higher by only 10%.

The results demonstrate the good convergence and high accuracy, obtained by PCGrate<sup>TM</sup> software and using profiles with polygonal random-roughness boundaries with 500 nodes and studied in the wide angular and spectral ranges. In simulations, we chose 1000 points of discretization per boundary and the „penetrating“ solver considering the finite conductivity of the grating material and disabled options of the convergence acceleration. The calculation error of  $\sim 0.001$  was evaluated from the energy balance taking into account rigorous calculations of the absorption [25]. The average time taken in both cases per a single calculation point at a portable workstation MSI<sup>®</sup> WT73VR 7RM with the processor Intel<sup>®</sup> Xeon<sup>®</sup> E3-1505M V6 & 4 GHz and 64 GB RAM, is  $\sim 1$  min under Windows<sup>®</sup> 10 Pro and the use of eightfold paralleling. Refractive indices of Au were taken from the website of CXRO [26].

## Conclusion

The technology of the mid-frequency blazed Si-gratings manufacturing was developed. Grating samples of



**Figure 6.** Theoretical diffraction efficiency of orders of the Au grating of 500 grooves/mm in the conical mount, calculated at a polar incidence angle of  $4^\circ$  and an azimuthal incidence angle of  $82^\circ$  using the actual groove profile, on wavelength.

500 grooves/mm with the blaze angle of  $\sim 4^\circ$ , the groove depth of  $\sim 130$  nm and working facet length of  $\sim 1800$  nm have the smooth profile, the grooves surface is clean, even, atomically smooth. The root-mean-square deviation of the surface roughness of the reflecting facets of Si gratings is 0.25–0.30 nm (measured in the field of  $1 \times 1 \mu\text{m}^2$ ). After coating of the Si-grating with the layer of Au, the RMS roughness increases almost twice; to reduce this parameter the additional studies are required. The rigorous diffraction efficiencies of the observed gratings reach unprecedented values of  $\sim 30\%$  and  $\sim 70\%$  in orders maximums in the SXR–EUV range in classical and conical grazing mounts of diffraction, respectively. Our further activities will be focused on the adaptation of the developed technology for manufacturing high-frequency gratings and studying their diffraction properties.

### Acknowledgements

The electron microscopic studies were performed using the equipment of the federal Common Research Center „Materials Science and Diagnostics in Advanced Technologies“ supported by the Ministry of Education and Science of Russia.

### Funding

The study is supported by the Russian Foundation for Basic Research (20-02-00326) in the experimental studies part. The study of L.I. Goray, K.Yu. Shubina, E.V. Pirogov and A.S. Dashkov is supported by the Russian Science Foundation (19-12-00270) in the theoretical part.

### Conflict of interest

The authors declare that they have no conflict of interest.

### References

- [1] L. Goray, W. Jark, D. Eichert. *J. Synchrotron Rad.*, **25**, 1683 (2018). DOI: 10.1107/S1600577518012419
- [2] L.I. Goray, G. Schmidt. *Boundary Integral Equation Methods for Conical Diffraction and Short Waves*, in *Gratings: Theory and Numerical Applications*, ed. by E. Popov, 2nd rev. ed. (Institut Fresnel, AMU, 2014), p. 447.
- [3] B.V. Egorov, S.Yu. Karpov, M.N. Mizerov. *J. Tech. Phys. (in Russian)* **54** (10), 1942 (1984).
- [4] P. Philippe, S. Valette, O. Mata Mendez, D. Maystre. *Appl. Opt.*, **24** (7) 1011 (1985). DOI: 10.1364/AO.24.001006

- [5] A.E. Franke, M.L. Schattenburg, E.M. Gullikson, J. Cottam, S.M. Kahn, A. Rasmussen. *J. Vac. Sci. Technol. B*, **15**, 2940 (1997). DOI: 10.1116/1.589759
- [6] I.Y. Yusupov, M.D. Mikhailov, R.R. Herke, L.I. Goray, S.B. Mamedov, O.A. Yakovuk. *Proc SPIE*, **1238**, 240 (1991). DOI: 10.1117/12.19398
- [7] D.L. Voronov, E.H. Anderson, R. Cambie, F. Salmassi, E.M. Gullikson, V.V. Yashchuk, H.A. Padmore, M. Ahn, C.-H. Chang, R.K. Heilmann, M.L. Schattenburg. *Proc. SPIE*, **7448**, 74480J (2009). DOI: 10.1117/12.826921
- [8] I. I. G., Inc. [Electronic source] Available at: URL: <http://pcgrate.com> (date of access 05.03.2021)
- [9] H. Seidel, L. Csepregi, A. Heuberger, H. Baumgartel. *J. Electrochem. Soc.*, **137** (11), 3612 (1990). DOI: 10.1149/1.2086277
- [10] U.D. Zeitner, T. Fugel-Paul, T. Harzendorf, M. Heusinger, E.-B. Kley. Talk [Electronic source] Available at: URL: <http://www.brera.inaf.it/DispersingElements2017/slides/Zeitner.pdf> (date of access 05.03.2021)
- [11] D.L. Voronov, E.M. Gulliskon, H.A. Padmore. *Opt. Express*, **25** (19), 23334 (2017). DOI: 10.1364/OE.25.023334
- [12] D.M. Miles, J.A. McCoy, R.L. McEntaffer, C.M. Eichfeld, G. Lavallee, M. Labella, W. Drawl, B. Liu, C.T. DeRoo, T. Steiner. *Astrophys. J.*, **869**, 95 (2018). DOI: 10.3847/1538-4357/aac73
- [13] C.-H. Chang, R.K. Heilmann, R.C. Fleming, J. Carter, E. Murphy, M.L. Schattenburg, T.C. Bailey, J.G. Ekerdt, R.D. Frankel, R. Voisin. *J. Vac. Sci. Technol. B*, **21** (6), 2755 (2003). DOI: 10.1116/1.1627814
- [14] D.L. Voronov, E.H. Anderson, R. Cambie, S. Cabrini, S.D. Dhuey, L.I. Goray, E.M. Gullikson, F. Salmassi, T. Warwick, V.V. Yashchuk, H.A. Padmore. *Opt. Express*, **19** (7), 6320 (2011). DOI: 10.1364/OE.19.006320
- [15] D.L. Voronov, S. Diez, P. Lum, S.A. Hidalgo, T. Warwick, N. Artemiev, H.A. Padmore. *Proc. SPIE*, **8848**, 88480Q (2013). DOI: 10.1117/12.2024489
- [16] M. Ahn, R.K. Heilmann, M.L. Schattenburg. *J. Vac. Sci. Technol. B*, **25** (6), 2593 (2007). DOI: 10.1116/1.2779048
- [17] L. Golub, P. Cheimets, E.E. DeLuca, C.A. Madsen, K.K. Reeves, J. Samra, S. Savage, A. Winebarger, A.R. Brucoleri. *J. Space Weather Space Clim.*, **10**, 37 (2020). DOI: 10.1051/swsc/2020040
- [18] M.S. Bibishkin, N.I. Chkhalo, A.A. Fraerman, A.E. Pestov, K.A. Prokhorov, N.N. Salashchenko, Yu.A. Vainer. *Nucl. Instrum. Meth. A*, **543**, 333 (2005). DOI: 10.1016/j.nima.2005.01.251
- [19] D.L. Voronov, P. Gawlitza, R. Cambie, S. Dhuey, E.M. Gullikson, T. Warwick, S. Braun, V.V. Yashchuk, H.A. Padmore. *J. Appl. Phys.*, **111**, 093521 (2012). DOI: /10.1063/1.4710985
- [20] J.A. McCoy, R.L. McEntaffer, D.M. Miles. *Astrophys. J.*, **891**, 114 (2020). DOI: 10.3847/1538-4357/ab76d3
- [21] A.V. Vinogradov, I.A. Brytov, A.Ya. Grudsky, M.T. Kogan, I.V. Kozhevnikov, V.A. Slemzin. *Zerkal'naya rentgenovskaya optika*, pod obshch. red. A.V. Vinogradova (Mashinostroenie, L., 1989), 464 s. (in Russian).
- [22] D.L. Voronov, M. Ahn, E.H. Anderson, R. Cambie, C.-H. Chang, L.I. Goray, E.M. Gullikson, R.K. Heilmann, F. Salmassi, M.L. Schattenburg, T. Warwick, V.V. Yashchuk, H.A. Padmore. *Proc. SPIE*, **7802**, 780207 (2010). DOI: 10.1117/12.861287
- [23] L. Goray, M. Lubov. *J. Appl. Cryst.*, **46**, 926 (2013). DOI: 10.1107/S0021889813012387
- [24] NTEGRA-Aura SPM. NT-MDT BV [Electronic source] Available at: URL: <https://ntmdt.nl/home/products/ntegra-aura/> (access date 05.03.2021).
- [25] L. Goray. *J. Synchrotron Rad.*, **28**, 196 (2021). DOI: <https://doi.org/10.1107/S160057752001440X>
- [26] Center of X-ray Optics [Electronic source] Available at: URL: <http://henke.lbl.gov/> (access date 05.03.2021).